



TECHNICAL ARTICLE

High-Velocity Oxygen Fuel-Sprayed WC-10Co4Cr Coatings on AISI 4135 Steel Substrate: Tensile and Fatigue Properties

Yong-kuan Zhou, Jia-jie Kang, Wen Yue, Tian-yang Yue, Zhi-qiang Fu, Li-na Zhu, and Ding-shun She

Submitted: 8 November 2021 / Revised: 26 April 2022 / Accepted: 21 May 2022 / Published online: 19 July 2022

In most studies of WC-based cermet coatings, attention has been given to the erosion, corrosion and wear resistance of the coatings. However, there have been a few studies highlighting the effect of spray WC-based cermet coating on the mechanical properties of the coating system. In this paper, AISI 4135 steel was used as the substrate to prepare WC-10Co4Cr coating by High-Velocity Oxygen Fuel technology (HVOF), and the tensile and fatigue properties of the HVOF-sprayed WC-10Co4Cr coating system were studied. This study showed that the WC-10Co4Cr coating degraded the tensile properties of the coating system, and with thicker coatings, this trend was more obvious. In addition, the fatigue life under different loads of the coating system was declined by spraying WC-10Co4Cr coating.

Keywords coating system, fatigue, HVOF, tensile, WC-10Co4Cr coating

1. Introduction

The AISI 4135 steel as a high strength, low-alloy steel is widely used in the manufacture of important structural parts in various equipment that bear impact, bending, torsion and high load (Ref 1-3). The WC-10Co4Cr cermet protective coatings with excellent erosion, corrosion and wear resistance prepared by HVOF technology are widely used in aerospace, metallurgy, ship, drilling and other fields (Ref 4-6).

In the actual service state, the structural parts sprayed by the WC-10Co4Cr coating are not only subjected to erosion, corrosion and wear (Ref 4, 7, 8), but also subjected to alternating loads, tension and compression, etc., which are likely to cause the parts to fail, thereby seriously reducing their service life. Therefore, while concerning and solving the

erosion, corrosion and wear resistance of the coating, it is necessary to research the influence of applied load on the tensile/fatigue properties of HVOF-sprayed WC-10Co4Cr coating on AISI 4135 steel.

A Koutsomichalis et al. (Ref 9) studied the tensile properties of the HVOF-sprayed WC-CoCr coatings on aluminum. The WC-CoCr coating decreased the tensile strength of the substrate. Besides, the transverse cracks were found to initiate on the surface of coating, increasing with the increase in tensile strain and stopped at the coating–substrate interface.

Different sandblasting processes have different effects on the fatigue life of samples. Costa et al. (Ref 10) evaluated the influence of WC-10Co-4Cr coating deposited by HVOF on the fatigue strength of Ti-6Al-4 V alloy. It was observed that the WC-10Co4Cr coating sprayed by HVOF technology reduced the fatigue strength of Ti-6Al-4 V alloy, and the influence was more significant in high cycle fatigue tests. However, the shot peening pre-treatment enhanced the fatigue life of coated Ti-6Al-4 V alloy by delaying crack nucleation and propagation. However, according to the theoretical analysis of thermal spraying, sandblasting pretreatment of the substrate can effectively improve the bonding strength of the coating and the substrate. Some studies showed that sandblasting pretreatment could cause surface defects and stress concentration on the substrate, which was prone to fatigue cracks. However, the residual compressive stress inside the HVOF-sprayed WC-CoCr coatings and the dense internal structure of the coatings would offset this negative effect. Therefore, the fatigue resistance of the samples prepared with WC-CoCr coatings on the surface did not deteriorate due to the sandblasting pretreatment (Ref 11, 12).

H.J.C. Voorwald et al. (Ref 13) compared the WC-17Co and WC-10Co-4Cr coatings applied by HVOF process and hard chromium electroplating on the fatigue strength of AISI 4340 steel. The results showed that compared with hard chromium electroplated, the tungsten carbide thermal spray coating had higher fatigue strength. J. R. Garcia et al. (Ref 14) found that the resistance to rotating bending fatigue in the HVOF-coated

Yong-kuan Zhou and **Tian-yang Yue**, School of Engineering and Technology, China University of Geosciences (Beijing), Beijing 100083, People's Republic of China; **Jia-jie Kang**, School of Engineering and Technology, China University of Geosciences (Beijing), Beijing 100083, People's Republic of China; Institute of Flexible Electronics Technology of Tsinghua. Zhejiang, Jiaxing 314000, People's Republic of China; Zhengzhou Institute, China University of Geosciences (Beijing), Zhengzhou 451283, People's Republic of China; and State Key Laboratory of Tribology, Department of Mechanical Engineering, Tsinghua University, Beijing 100084, People's Republic of China; and **Wen Yue**, **Zhi-qiang Fu**, **Li-na Zhu**, and **Ding-shun She**, School of Engineering and Technology, China University of Geosciences (Beijing), Beijing 100083, People's Republic of China; and Zhengzhou Institute, China University of Geosciences (Beijing), Zhengzhou 451283, People's Republic of China. Contact e-mail: kangjjjie@cugb.edu.cn.

test samples was stronger than in the uncoated material. Due to a larger elasticity module, the WC coating bore more stress than the steel under the same deformation. However, once the fatigue cracks initiated in the coatings, the growth rate was faster, and it was more likely to cause fracture damage. Villalobos-Gutiérrez et al. (Ref 15) investigated the fatigue behavior of AA6063-T6 aluminum alloy coated with WC-10Co-4Cr alloy deposited by HVOF thermal spraying. Compared with uncoated substrate, the fatigue life of coated aluminum alloy was significantly improved when testing in air and 3 wt. % NaCl solution. The fatigue cracks nucleated at the surface of coating first and then propagated toward the substrate. J. G. L Barbera Sosa et al. (Ref 16) used HVOF spraying technology to prepare a composite coating of 50% WC-CoCr and 50% NiWCrSiFeB. The results showed that the stress concentration occurred at the interface with the substrate, which would induce the initiation and propagation of fatigue cracks, thereby reducing the fatigue life of the coated samples.

Finite element software has been widely used in material simulation, which reduces the amount of experimentation effectively (Ref 17). Finite element meshes were constructed on SEM micrographs of HVOF-sprayed WC-CoCr, and the micro-scale elastic modulus value obtained from the uniaxial tensile test simulated on high-magnification micrographs is consistent with the experimental result. The results showed that under actual applied loads, failure will first occur in stress concentration area in WC particles where oxide inclusions are more abundant (Ref 18). U. A. Ozden et al. (Ref 19) used Abaqus to simulate the fatigue fracture of WC-Co. The WC and Co phases had different failure mechanism due to different elastic modulus. Besides, they also simulated a more accurate geometric structure based on the microstructure of the material, and the simulation results were similar to the test results and had good consistency with the actual fracture path (Ref 20).

The fatigue life of the thermal-sprayed component can be affected by the residual stresses from coating deposition, which includes torch processing parameters and deposition effects. Andrew Vackel et al. (Ref 21) investigated influence of process and deposition parameters on the fatigue behavior of thermal spraying WC-CoCr-steel system. The results indicate that compressive residual stress of coating delayed the damage of the substrate, enabling fatigue strength of the coated component. The size and population of porosities in the coating had effects on fatigue strength. Because the fatigue crack initiated at the porosities, therefore the larger and more porosities, the lower fatigue strength (Ref 22). Chandra, N. P. S. et al. (Ref 23) studied the effect of coating thickness on fatigue strength. When the coating was excessively thick, higher tensile residual stress occurred near the coating and substrate interface. Nevertheless, when the coating was too thin, the deformation of substrate crystal would aggravate the fracture of coating.

There are few studies on the tensile and fatigue properties of the coating system (composed of HVOF-sprayed WC-10Co4Cr coatings on AISI 4135 steel substrate); the main purpose of this research is to analyze the effect of spraying WC-10Co4Cr coating on the tensile and fatigue properties of the coating system. Universal testing machine was used for the tensile test of the coating system, and high-frequency fatigue testing machine was used for the fatigue test. The residual stress was tested by x-ray diffraction (XRD). The elastic modulus of the

coating and substrate was measured by Nano Indenter. The fracture morphologies of the coating system were observed by Scanning electron microscope (SEM). Details on the tensile and fatigue properties of the coating system were discussed in later sections.

2. Experimental Procedure

2.1 Coating Preparation

Commercial WC-10Co4Cr bimodal composite powder (produced by BGRIMM Technology Group) was selected as the raw material, and the chemical composition of the powder is WC-86 wt %, Co-10 wt %, and Cr-4 wt. %. The particle size of the powder is 15–40 μm . The mass ratio of micron WC particles and nanosized WC particles in the powder is 7:3. The size of micron WC particles is 0.7 ~ 1.3 μm , and the size of nanoscale WC particles is 70 ~ 200 nm. AISI 4135 steel was selected as the substrate, and in order to ensure the good mechanical properties of the substrate, the substrate was quenched at 850 °C and tempered at 550 °C. The chemical composition of AISI 4135 steel is as follows: C: 0.18-0.40, Cr: 0.80-1.10, Mo: 0.15-0.25, Mn: 0.40-0.70, Si: 0.17-0.37, and balance Fe.

The GTV MF-P-HVF-K 2000 HVOF system equipped with GTV HVOF K2 spray gun was used for spraying coating. With aviation kerosene as fuel, oxygen as combustion gas and nitrogen as powder carrier, the HVOF spraying process parameters are shown in Table 1. Before spraying, AISI 4135 steel substrate was cleaned in ultrasonic equipment by acetone for 30 min to remove oil and clean. In order to increase the compressive stress and ensure the better combination of the coating and the substrate, sand blasting was roughened. The pressure of compressed air using for the sand blasting was 0.5 MPa. The sand blasting material was corundum with a size of 0.3 mm, and the distance and angle of sand blasting were 300 mm and 70°, respectively.

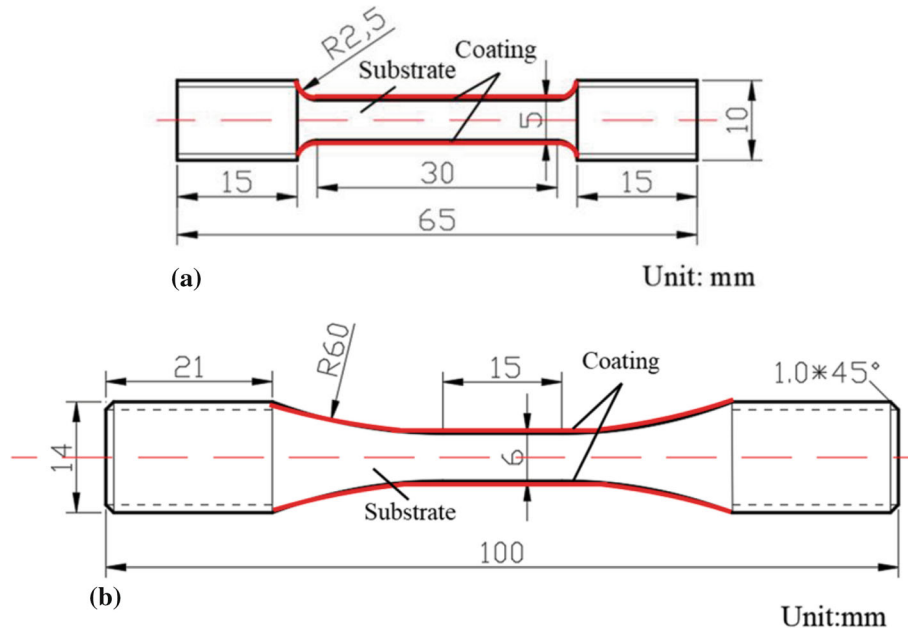
2.2 Tensile and Fatigue Tests

The Instron 5985 electronic universal testing machine was used to conduct tensile test of the coating system, and the influence of different thickness of the coating on the tensile properties of the coating system was discussed. The tensile test temperature was room temperature (25 °C), and the tensile rate was 1.8 mm/min. The tensile test specimens are shown in Fig. 1(a). In order to prevent stress concentration, a certain radian was set, and the sample was held for rotary spraying. The diameters of the substrate parts are 5 mm, and the coating can be divided into two types: 140 μm and 280 μm .

The coating system was subjected to fatigue test by QBG-100 high-frequency fatigue tester. The diameter of the substrate part was 6 mm, and the coating system was all polished to reduce the roughness to $R_a < 10 \mu\text{m}$, and the thickness of the coating after polishing was about 100 μm . The fatigue test specimens are shown in Fig. 1(b). The coating was subjected to axial loading at room temperature with stress ratio $R = 0.1$. Loading frequency was 100 Hz, and the specified conditional fatigue life was 10^6 circles. According to the axial loading

Table 1 Process parameters of HVOF spraying WC-10Co4Cr coating

Process parameters	Powder feed rate	Spray distance	Oxygen flow rate	Kerosene flow rate	Nitrogen flow rate
Value	100 g·min ⁻¹	420 mm	902 L·min ⁻¹	26 L·min ⁻¹	9 L·min ⁻¹

**Fig. 1** Dimensions of test specimens. (a) Tensile test; (b) fatigue test

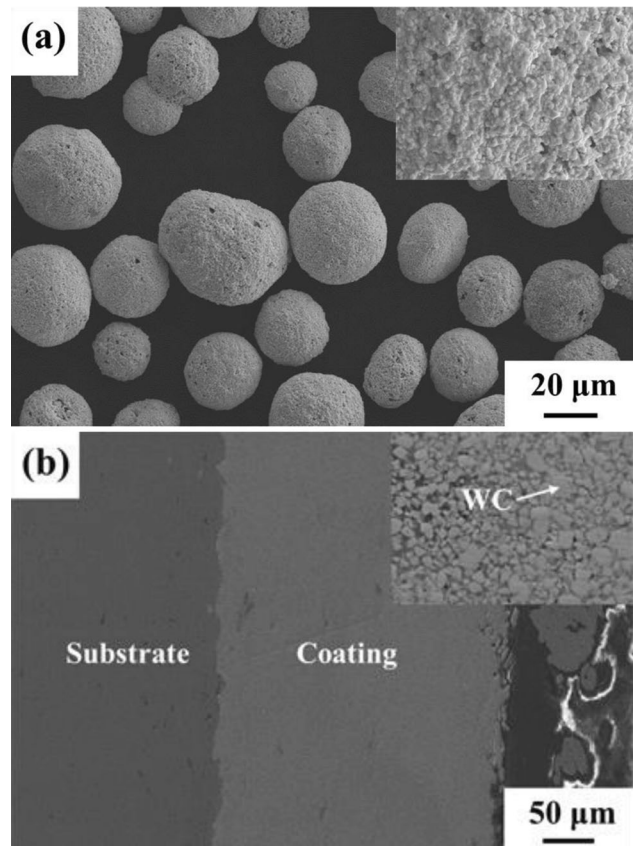
fatigue test standard of HB5287-96, the conditional fatigue limit of the coating system was tested by the four-stage lifting method, and the fatigue life of the coating system under overload was measured by the group method. The conditional fatigue limit of the material is determined by lifting method. The stress increment is generally within 5% of the predicted fatigue limit, and the test can be carried out at grade 3 ~ 5 stress levels. In this paper, four-stage stress level was used, which was called the four-stage lifting method. The fatigue life under overloads was measured by group method. The quantity distribution of the coating system at all stress levels should increase gradually with the decrease in stress levels. The conditional fatigue limit obtained by lifting method was regarded as the lowest stress level point on S-N curve.

The morphologies of the coating system were examined by ZEISS MERLIN Compact scanning electron microscope (SEM), including the WC-10Co4Cr powders, cross section, the fracture morphologies of tensile and fatigue specimens. Agilent Nano Indenter G200 was used to measure the elastic modulus of the coating, the load was 300 g, the duration was 20 s, and the average elastic modulus of the five tests was taken. In order to test the residual stress change of the coating system, Philips MRD 3710 x-ray diffraction was used to measure the residual stress of the coating system.

3. Results and Discussion

3.1 Morphologies of Powders and Coatings

Figure 2 shows the morphologies of the WC-10Co4Cr powders and coatings. The upper right corner of the figure is

**Fig. 2** Morphologies of the WC-10Co4Cr powders and coatings. (a) The powders; (b) The coatings

the enlarged figure. As can be seen in Fig. 2(a), the spray powders exhibit spherical or ellipsoidal shape, and the powder surface is loose and porous. Figure 2(b) shows the cross-sectional of the WC-10Co4Cr coatings; the WC-10Co4Cr coatings bind tightly to AISI 4135 steel substrate. Besides, the coatings have dense microstructure, which consist of block WC phase and CoCr bonding phase. In WC-CoCr cermet system, the WC phase has excellent hardness, and the CoCr phase is a good binder, both of which are indispensable (Ref 8).

3.2 Tensile Tests

Figure 3 shows the tensile stress–strain curves of the substrate and the coating system with different thickness at room temperature, and Table 2 shows the corresponding tensile test data. It can be seen that the yield strength, tensile strength and elongation after fracture of the coating system are lower than AISI 4135 substrate (952 MPa). The yield strength, tensile strength and elongation after fracture of the coating system (140 μm) are decreased by 7.8, 19.7; 68.0%, respectively. And the yield strength, tensile strength and elongation after fracture of the coating system (280 μm) decrease by 36.6%, 40.5%; 26.0%, respectively. Because AISI 4135 steel substrate is a plastic material, while the WC-10Co4Cr coating is a brittle

material, that plastic materials generally have greater fracture strain than brittle materials, so the tensile fracture failure of the coating occurs before the substrate, leading to a decrease in the tensile strength of the coating system, and the thicker the coating, the greater the proportion of the coating area in the coating system, the less the area can bear the load when it fails, and the more obvious the tensile strength of the coating system declines (Ref 9, 24, 25).

The coating can be treated as the composite material parallel to the substrate, and both the coating and the substrate are the components that determine the plasticity and brittleness. Since the strain applied in the axial direction is the same, it is assumed that the strain condition of the substrate and the coating is equal strain. According to the mixing law of composite materials, the calculation formula of elastic modulus of coating system is as follows: $E_{cs}A_s + A_c = E_cA_c + E_sA_s$, where E_{cs} , E_s , E_c are the elastic modulus of the coating system, the substrate and coating, respectively, and A_s , A_c are the area of the substrate and the coating. According to the nanoindentation experimental data, the average elastic modulus of AISI 4135 steel substrate is 193 ± 8 GPa, and the average elastic modulus of the coating is 318 ± 15 GPa. The elastic modulus of the coating system (140 μm) is 242 ± 10 GPa derived from

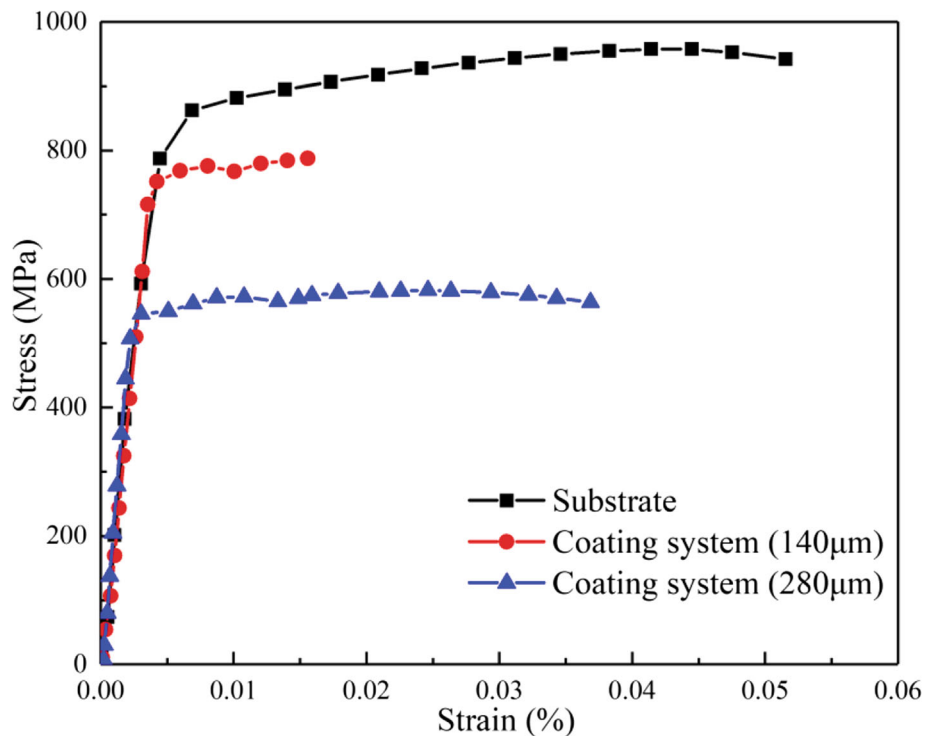


Fig. 3 Tensile stress–strain curves of the substrate and the coating system with different thickness

Table 2 Tensile properties of the substrate and the coating system with different thickness

Samples	Yield strength, MPa	Tensile strength, MPa	Elongation, mm/mm
4135 steel	797 ± 37	952 ± 50	0.050 ± 0.002
Coating system (140 μm)	735 ± 34	764 ± 43	0.016 ± 0.001
Coating system (280 μm)	505 ± 28	566 ± 27	0.037 ± 0.002

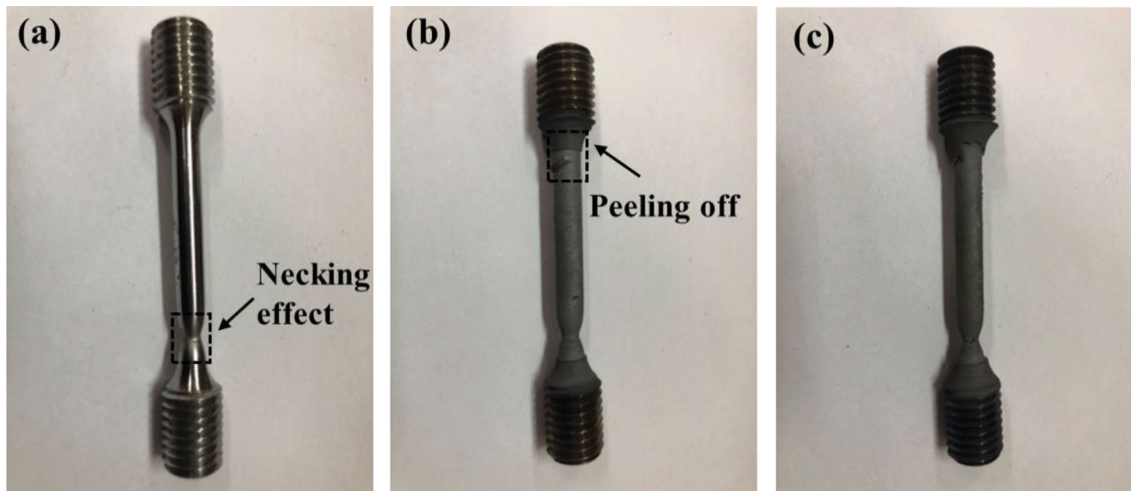


Fig. 4 Macro-morphologies of the substrate and the coating system with different thickness after the tensile test. (a) Substrate; (b) Coating system (140 μm); (c) Coating system (280 μm)

the stress–strain curve. The elastic modulus of the coating system is 234 GPa (140 μm), which is estimated according to the formula. The tensile test value is in good agreement with the theoretical calculated value.

It can be seen from Fig. 4 that the substrate and the coating system with different thickness all have obvious plastic deformation. In the process of tensile, strain hardening cannot keep pace with the development of plastic deformation, so deformation and necking occur at a stress concentration point in the tensile area. In the initial stage of the tensile, WC-10Co4Cr coating can keep consistent with substrate deformation; however, due to the stiffness of the coating is far greater than the substrate, the coating will exfoliate when the stress value exceeds the allowable limit of the coating during the tensile test (Ref 26), and the thicker the coating is, the more thoroughly it exfoliates.

Figure 5 shows the fracture morphologies of the substrate and the coating system with different thickness. As can be seen from Fig. 5(a), AISI 4135 steel substrate presents the morphology of ductile fracture, and the fracture area can be divided into typical fiber zone, radical zone and shear lip. The fracture features in the fiber zone are dimples, and the microscopic fracture features in the radical zone are cleavage steps Fig. 5(d) and (e). From Fig. 5(b) and (c), as for the coating system, the coating is brittle material and the substrate is plastic material. The thicker the coating is, the smaller the fiber zone, and the worse the plasticity of the coating system (Ref 27, 28). When the concentrated stress of the coating system exceeds the allowable limit of the coating in the tensile test, the coating will crack. With the increase in the tensile stress, the coating system will fracture eventually.

Figure 6 shows the micro-morphologies of the unfractured tensile specimens. Figure 6(a) and (b) shows the side-section of coating systems with different thickness. The brittle fracture of the coating occurs under the action of tensile load. Multiple cracks appear on the surface of the coating perpendicular to the tensile direction and parallel to each other. This is because the addition of brittle coating changes the stress distribution of

AISI 4135 steel substrate in the tensile direction. The interaction between WC hard phases in the coating results in stress concentration, so WC particles becomes the crack initiation point in the coating. Under the condition of tensile stress, the brittle cracking of the coating leads to the initiation of surface cracks. As can be seen from Fig. 6(c) and (d), when the crack density reaches saturation, the continuous increase in tensile stress will lead to the internal diffusion of cracks along the CoCr bonding phase, and the penetration cracks of the coating will occur, thus leading to the failure of the coating system. The ability of the coating to bear the load after cracking is greatly reduced so that it can be ignored, which also leads to the decline of the yield strength of the coating system, which is consistent with the phenomenon described in Fig. 4. In addition, it can be seen from Fig. 6(e) that the coating is exfoliated from the substrate.

3.3 Fatigue Tests

Figure 7 shows the conditional fatigue limit curve of the substrate and the coating system. After calculation, the conditional fatigue limit $\sigma_{R(10^6)}$ of the substrate is 712.5 MPa, and that of the coating system is 682.5 MPa, which is lower than that of the uncoated sample. This is because the coating is also subjected to tensile load in the fatigue test, while the WC-10Co4Cr coating is brittle material and will fail rapidly under tensile stress. Considering that the coating cracks under tensile load, its loadbearing capacity drops significantly (it probably becomes negligible) as soon as the cracks are formed. Besides, the effect of sprayed coating on the residual stress of the coating system is complex. On the one hand, the residual compressive stress on the surface of AISI 4135 steel after sandblasting before HVOF process decreases the notch stress concentration factor and fatigue notch sensitivity; thus, the fatigue life of the coating system is improved (Ref 29). But it should be noted that sandblasting process must be controlled; otherwise, sandblasting particles may cause damage to the

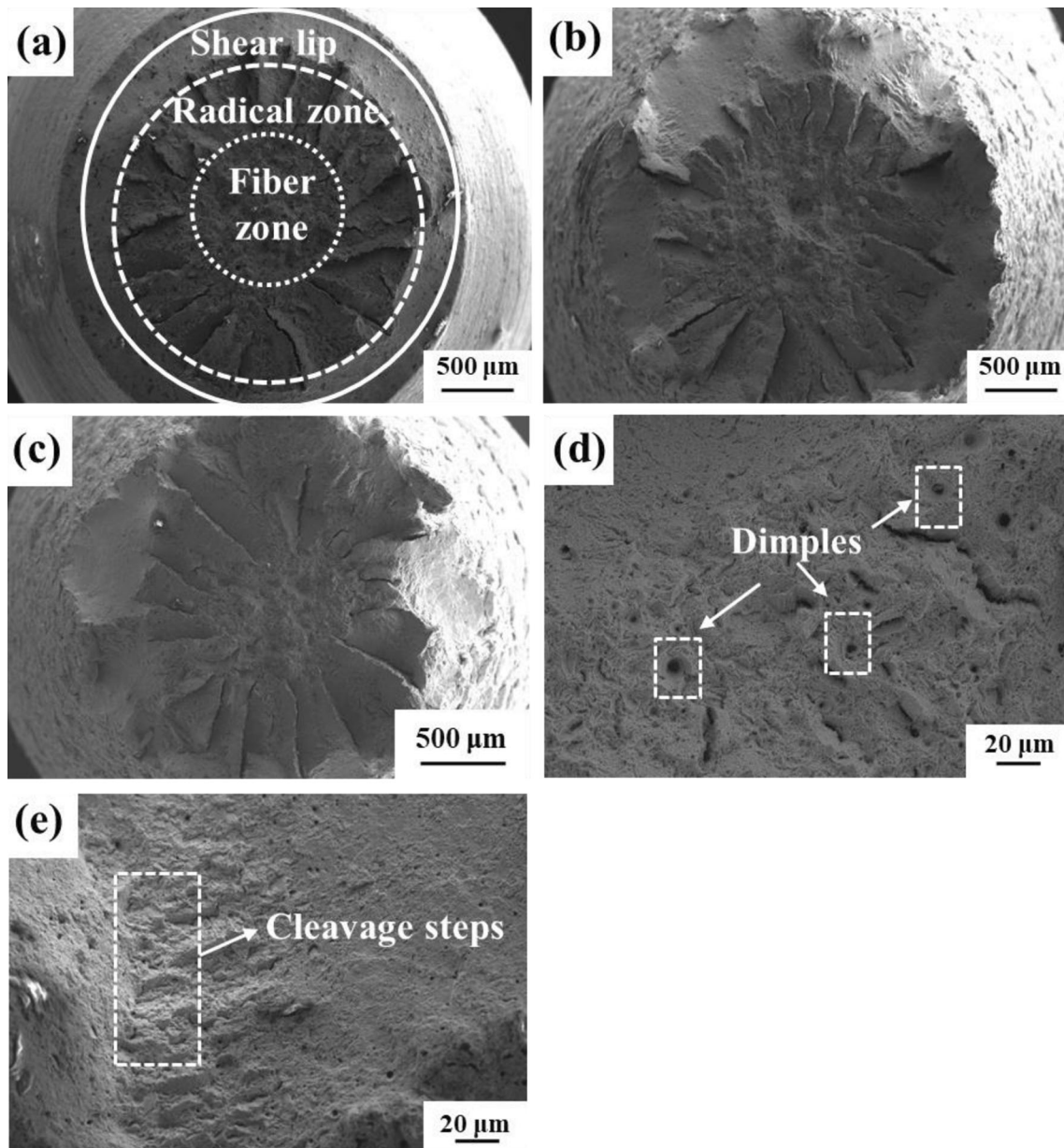


Fig. 5 Micro-morphologies of the fractured tensile specimens. (a) Substrate; (b) Coating system (140 μm); (c) Coating system (280 μm); (d) Dimples; (e) Cleavage steps

substrate surface, thereby reducing fatigue life of the substrate (Ref 11). On the other hand, spraying coating will produce impact effect and thermal stress on the coating system in the spraying process. The impact effect leads to compressive stress on the coating system, and the thermal stress is tensile stress. The final stress state depends on the comprehensive action of compressive stress and tensile stress. The average residual stress of the coating system is -152 ± 10 MPa, showing compressive stress state, which can restrain the crack growth and is beneficial to the fatigue life (Ref 13, 30).

Figure 8(a) shows the S-N logarithmic fatigue life comparison of the substrate and the coating system under overload conditions. According to the conditional fatigue limit obtained by the four-stage lifting method, the fatigue overloads are 700,

735, 770, 820 and 870 MPa, respectively. It can be seen that the fatigue life of the coating system is significantly lower than that of the substrate. This is also caused by the brittleness of the coating, which is difficult to bear the cyclic alternating stress, resulting in the decline of the fatigue life of the coating system.

Figure 9 shows the typical fatigue fracture of coating system with different cycles. It can be seen from Fig. 9(a) that the crack source of the coating system is mainly generated at the interface between the coating and the substrate, and then expands along the interface or deviates from the interface toward the coating (Ref 23, 31). The coating and substrate separation occurs, resulting in coating failure, as shown in Fig. 9(b) and (d). Crack sources also form cleavage steps along the substrate after initiation at the interface, as shown in

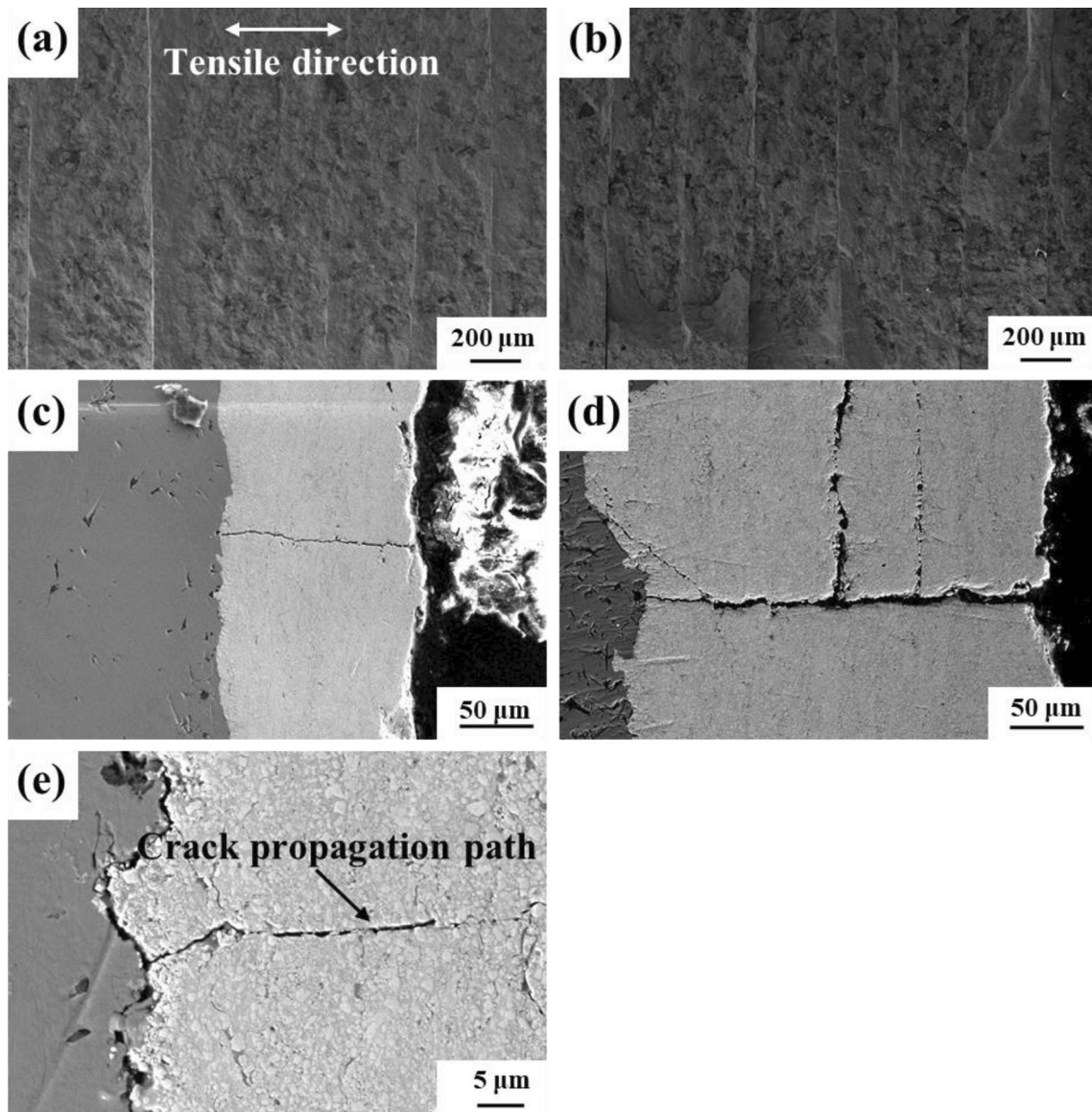


Fig. 6 Micro-morphologies of the unfractured tensile specimens. (a) Side-section of coating system (140 μm); (b) Side-section of coating system (280 μm); (c) Cross section of coating system (140 μm); (d) Cross section of coating system (280 μm); (e) Crack propagation path

Fig. 9(c). Such cracks may reduce the fatigue life of AISI 4135 steel substrate.

4. Conclusion

In this paper, the universal testing machine was used to carry out tensile test on the substrate and the coating system, and the fatigue testing machine was used to carry out fatigue test on the coating system. The failure form of the samples was judged by observing the fracture morphologies, and then, the tensile and fatigue properties of the coating system were explored, and the following main conclusions were drawn.

(1) The existence of WC-10Co4Cr coating results in a decrease in the yield strength, tensile strength and elongation after fracture of the coating system, and this phenomenon is more obvious with the thickness of the coating. The decrease in the tensile property of the coating system is related to the brittleness of the coating. Compared with the coating of different thickness, the 280 μm coating is more serious than the 140 μm coating.

(2) The fatigue crack source of the coating system mainly occurs at the interface between the coating and the substrate and then, expands along the interface or deviates from the interface to the coating. Crack sources also form cleavage steps along the substrate after initiation at the interface. Such cracks

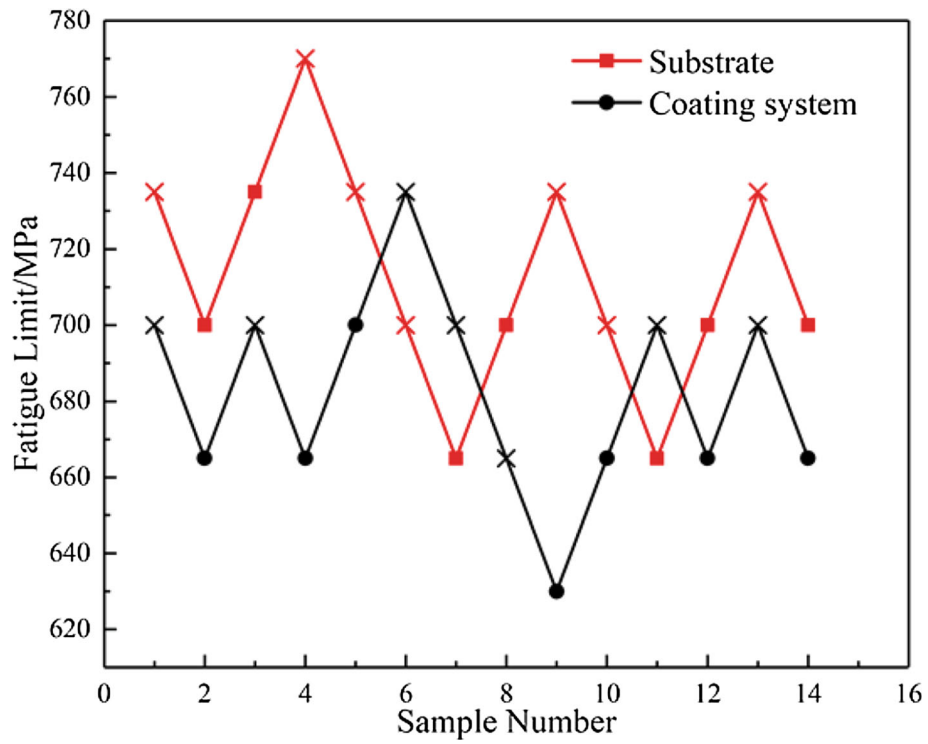


Fig. 7 Conditional fatigue limit $\sigma_{0.1}$ for four-level stress level test method of the substrate and the coating system

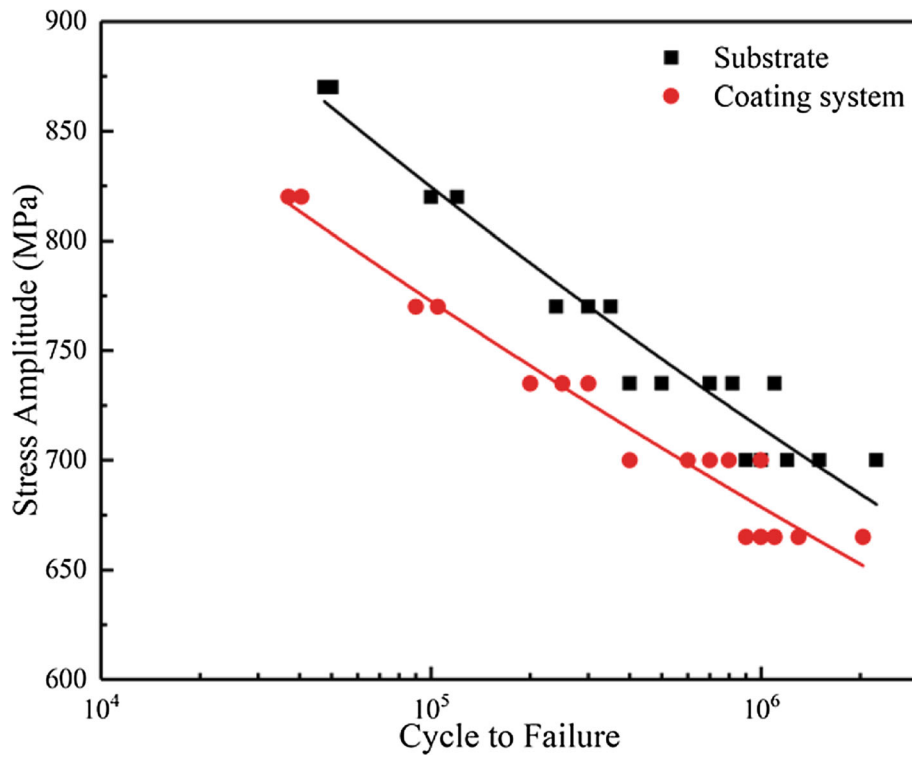


Fig. 8 Simulated S-N curves of the substrate and the coating system with maximum likelihood method

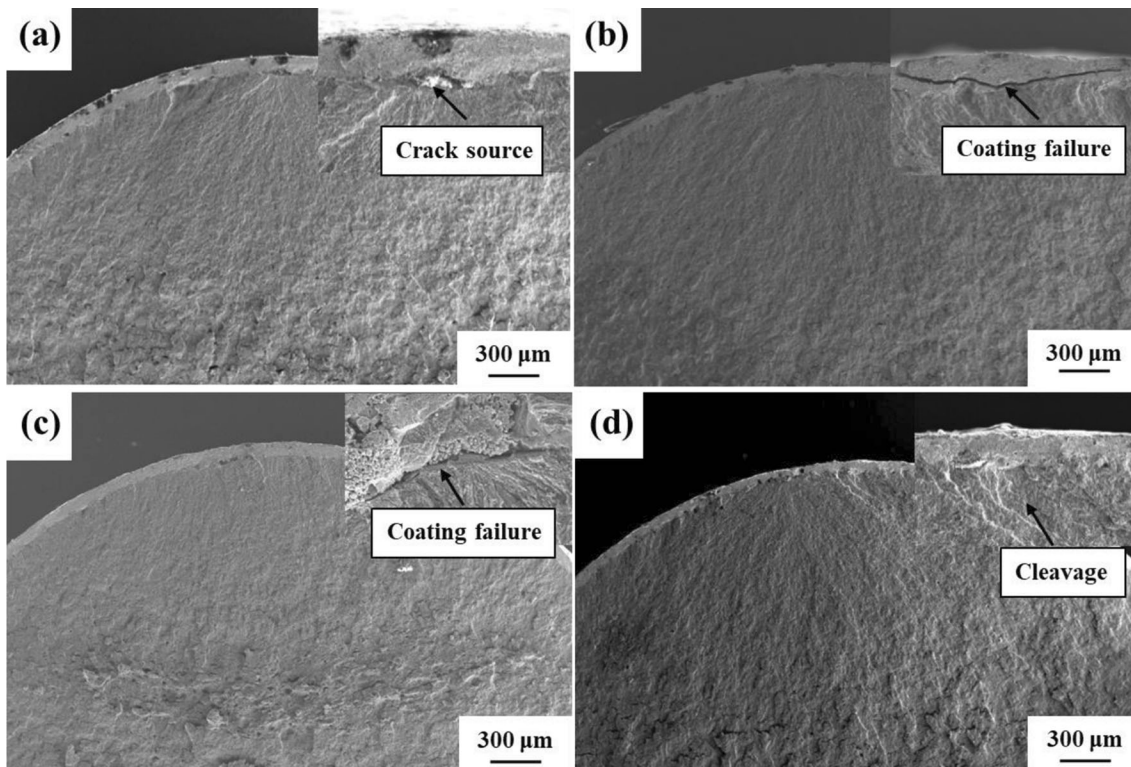


Fig. 9 Fatigue fracture morphologies of the coating system. (a) Crack source; (b, c) Coating failure; (d) Cleavage

may reduce the fatigue life of AISI 4135 steel substrate. The fatigue life of the coating system is declined by spraying WC-10Co4Cr coating under different loads.

Acknowledgments

The authors gratefully acknowledge the National Natural Science Foundation of China (Grant Number 52175196), the Pre-Research Program in National 14th Five-Year Plan (Grant Number 61409230614), and the Fundamental Research Funds for Central Universities (Grant Numbers 265QZ2021008, 2652019069).

References

1. A.L. Marcelo, A.Y. Uehara, R.M. Utiyama and I. Ferreira, Fatigue Properties of High Strength Bolts, *Procedia Eng.*, 2011, **10**, p 1297–1302.
2. W. Qu, Y. Huang, X. Yu, D. Lu, M. Zheng and R. De Marco, Effect of Heat Treatment on Hydrogen Permeation Behaviour of AISI 4135 Steel Under Splash Zone Conditions, *Corros. Eng. Sci. Technol.*, 2016, **51**(3), p 163–170.
3. W. Yue, X.C. Gao, Y.D. Liu, X.J. Sun, C.B. Wang and J.J. Liu, Tribological Properties of Sulfurized-Nitrided Layer Prepared by a Two-Step Method, *Vacuum*, 2011, **85**(11), p 1011–1016.
4. S. Hong, Y.P. Wu, W.W. Gao, J.F. Zhang, Y.G. Zheng and Y. Zheng, Slurry Erosion-Corrosion Resistance and Microbial Corrosion Electrochemical Characteristics of HVOF Sprayed WC-10Co-4Cr Coating for Offshore Hydraulic Machinery, *Int. J. Refract. Met. Hard Mat.*, 2018, **74**, p 7–13.
5. Y. Tian, H.J. Zhang, X.Y. Ghen, A. McDonald, S.J. Wu, T.H. Xiao and H. Li, Effect of Cavitation on Corrosion Behavior of HVOF-Sprayed WC-10Co4Cr Coating with Post-Sealing in Artificial Seawater, *Surf. Coat. Technol.*, 2020, **397**, 126012.
6. S.G. Sapate, N. Tangselwar, S.N. Paul, R.C. Rathod, S. Mehar, D.S. Gowtam and M. Roy, Effect of Coating Thickness on the Slurry Erosion Resistance of HVOF-Sprayed WC-10Co-4Cr Coatings, *J. Therm. Spray Technol.*, 2021, **30**(5), p 1365–1379.
7. H.B. Wang, X.Z. Wang, X.Y. Song, X.M. Liu and X.W. Liu, Sliding Wear Behavior of Nanostructured WC-Co-Cr Coatings, *Appl. Surf. Sci.*, 2015, **355**, p 453–460.
8. Y.K. Zhou, X.B. Liu, J.J. Kang, W. Yue, W.B. Qin, G.Z. Ma, Z.Q. Fu, L.N. Zhu, D.S. She, H.D. Wang, J. Liang, W. Weng and C.B. Wang, Corrosion Behavior of HVOF Sprayed WC-10Co4Cr Coatings in the Simulated Seawater Drilling Fluid Under the High Pressure, *Eng. Fail. Anal.*, 2020, **109**, 104338.
9. A. Koutsomichalis, M. Vardavoulias and N. Vaxevanidis, HVOF Sprayed WC-CoCr Coatings on Aluminum: Tensile and Tribological Properties, *IOP Conf. Ser. Mater. Sci. Eng.*, 2017, **174**, p 012062. <https://doi.org/10.1088/1757-899X/174/1/012062>
10. M.Y.P. Costa, M.L.R. Venditti, H.J.C. Voorwald, M.O.H. Cioffi and T.G. Cruz, Effect of WC-10%Co-4%Cr Coating on the Ti-6Al-4V Alloy Fatigue Strength, *Mater. Sci. Eng. A-Struct. Mater. Prop. Microstruct. Process.*, 2009, **507**(1–2), p 29–36.
11. W.A. Gonzalez-Hermosilla, D. Chicot, J. Lesage, J.G. La Barbera-Sosa, I.C. Gruescu, M.H. Staia and E.S. Puchi-Cabrera, Effect of Substrate Roughness on the Fatigue Behavior of a SAE 1045 Steel Coated with a WC-10Co-4Cr Cermet, Deposited by HVOF Thermal Spray, *Mater. Sci. Eng. A-Struct. Mater. Prop. Microstruct. Process.*, 2010, **527**(24–25), p 6551–6561.
12. E.S. Puchi-Cabrera, M.H. Staia, Y.Y. Santana, E.J. Mora-Zorrilla, J. Lesage, D. Chicot, J.G. La Barbera-Sosa, E. Ochoa-Perez and C.J. Villalobos-Gutierrez, Fatigue Behavior of AA7075-T6 Aluminum Alloy Coated with a WC-10Co-4Cr Cermet by HVOF Thermal Spray, *Surf. Coat. Technol.*, 2013, **220**, p 122–130.
13. H.J.C. Voorwald, R.C. Souza, W.L. Pigatin and M.O.H. Cioffi, Evaluation of WC-17Co and WC-10Co-4Cr Thermal Spray Coatings by HVOF on the Fatigue and Corrosion Strength of AISI 4340 Steel, *Surf. Coat. Technol.*, 2005, **190**(2–3), p 155–164.
14. J.R. Garcia, J.E. Fernandez, J.M. Cuertos and F.G. Costales, Fatigue Effect of WC Coatings Thermal Sprayed by HVOF and Laser Treated, on Medium Carbon Steel, *Eng. Fail. Anal.*, 2011, **18**(7), p 1750–1760.

15. C.J. Villalobos-Gutierrez, G.E. Gedler-Chacon, J.G. La Barbera-Sosa, A. Pineiro, M.H. Staia, J. Lesage, D. Chicot, G. Mesmacque and E.S. Puchi-Cabrera, Fatigue and Corrosion Fatigue Behavior of an AA6063-T6 Aluminum Alloy Coated with a WC-10Co-4Cr Alloy Deposited by HVOF Thermal Spraying, *Surf. Coat. Technol.*, 2008, **202**(18), p 4572–4577.
16. J.G. La Barbera-Sosa, Y.Y. Santana, C. Villalobos-Gutierrez, D. Chicot, J. Lesage, X. Decoopman, A. Iost, M.H. Staia and E.S. Puchi-Cabrera, Fatigue Behavior of a Structural Steel Coated with a WC-10Co-4Cr/Colmonoy 88 Deposit by HVOF Thermal Spraying, *Surf. Coat. Technol.*, 2013, **220**, p 248–256.
17. A. Vackel, T. Nakamura and S. Sampath, Mechanical Behavior of Spray-Coated Metallic Laminates, *J. Therm. Spray Technol.*, 2016, **25**(5), p 1009–1019.
18. G. Bolelli, A. Candelì, H. Koivuluoto, L. Lusvarghi, T. Manfredini and P. Vuoristo, Microstructure-Based Thermo-Mechanical Modelling of Thermal Spray Coatings, *Mater. Des.*, 2015, **73**, p 20–34.
19. U.A. Özden, A. Bezold and C. Broeckmann, Numerical Simulation of Fatigue Crack Propagation in WC/Co Based on a Continuum Damage Mechanics Approach, *Procedia Mater. Sci.*, 2014, **3**, p 1518–1523.
20. U.A. Oezden, K.P. Mingard, M. Zivcec, A. Bezold and C. Broeckmann, Mesoscopical Finite Element Simulation of Fatigue Crack Propagation in WC/Co-Hardmetal, *Int. J. Refract. Met. Hard Mat.*, 2015, **49**, p 261–267.
21. A. Vackel and S. Sampath, Fatigue behavior of thermal sprayed WC-CoCr- steel systems: Role of process and deposition parameters, *Surf. Coat. Technol.*, 2017, **315**, p 408–416.
22. H. Akebono, J. Komotori and M. Shimizu, Effect of Coating Microstructure on the Fatigue Properties of Steel Thermally Sprayed with Ni-Based Self-Fluxing Alloy, *Int. J. Fatigue*, 2008, **30**(5), p 814–821.
23. N.P.S. Chandra, Y. Otsuka, Y. Mutoh and K. Yamamoto, Effect of Coating Thickness on Fatigue Behavior of TiAlN Coated Ti-Alloys, *Int. J. Fatigue*, 2020, **140**, 105767.
24. G.M. Smith, O. Higgins and S. Sampath, In-Situ Observation of Strain and Cracking in Coated Laminates by Digital Image Correlation, *Surf. Coat. Technol.*, 2017, **328**, p 211–218.
25. M. Gui, R. Eybel, B. Asselin and F. Monerie-Moulin, Cracking and Spalling Behavior of HVOF Thermally Sprayed WC-Co-Cr Coating in Bend and Axial Fatigue Tests, *J. Mater. Eng. Perform.*, 2015, **24**(3), p 1–10.
26. Z.B. Chen, Z.G. Wang and S.J. Zhu, Tensile Fracture Behavior of Thermal Barrier Coatings on Superalloy, *Surf. Coat. Technol.*, 2011, **205**(15), p 3931–3938.
27. P. Li, J. Zhou, L. Li, T. Zhang, Y. Gou, X. Meng and J. Lyu, Tensile Fracture Behavior of 316L Stainless Steel Components Fabricated with Hybrid Directed Energy Deposition and Thermal Milling Manufacturing, *Appl. Phys. A*, 2021 <https://doi.org/10.1007/s00339-021-04381-4>
28. E. Azinpour, R. Darabi, J.C. de Sa, A. Santos, J. Hodek and J. Dzukan, Fracture Analysis in Directed Energy Deposition (DED) Manufactured 316L Stainless Steel Using a Phase-Field Approach, *Finite Elem. Anal. Des.*, 2020, **177**, 103417.
29. E. Hernandez-Rengifo, S.A. Rodriguez and J.J. Coronado, Improving Fatigue Strength of Hydromachinery 13Cr-4Ni CA6NM Steel with Nitriding and Thermal Spraying Surface Treatments, *Fatigue Fract. Eng. Mater. Struct.*, 2021, **44**(4), p 1059–1072.
30. T. Varis, T. Suhonen, J. Laakso, M. Jokipii and P. Vuoristo, Evaluation of Residual Stresses and their Influence on Cavitation Erosion Resistance of High Kinetic HVOF and HVOF-Sprayed WC-CoCr Coatings, *J. Therm. Spray Technol.*, 2020, **29**(6), p 1365–1381.
31. V.P. Nguyen, T.N. Dang, C.C. Le and D.A. Wang, Effect of Coating Thickness on Fatigue Behavior of AISI 1045 Steel with HVOF Thermal Spray and Hard Chrome Electroplating, *J. Therm. Spray Technol.*, 2020, **29**(8), p 1968–1981.

Publisher's Note Springer Nature remains neutral with regard to jurisdictional claims in published maps and institutional affiliations.